International Journal Of
Industrial Electronics Control and Optimization
Print ISSN: 3517-2645
Online ISSN: 3568-2645
Homepage: https://ieco.usb.ac.ir/

Analysis of the Squirrel Cage Induction Motor in the Broken Rotor Bar Condition Based on the Calculation of the Rotor Bar Current

Hamed Shadfar, Hamid Reza Izadfar*

Faculty of Electrical and Computer Engineering Department, Semnan University, Semnan, Iran
Corresponding author's email: hrizadfar@semnan.ac.ir

Article Info

Article type:
Research Article

Article history:
Received: 25-May-2025
Received in revised form: 28-August-2025
Accepted: 01-September-2025
Published online: 21-March-2026

Keywords:
Broken rotor bar fault,
Multiple coupled circuit,
Rotor bar current,
Squirrel cage Induction motor.

ABSTRACT

Calculating the current of the rotor bars in a squirrel cage induction motor (SCIM) using stator data is difficult, but it is very useful. With the calculation of the rotor bars' current, analysis and investigation of various parameters of the motor can be conducted precisely. One of the faults faced by SCIM is the broken rotor bar (BRB) fault. The breakage of one or more bars causes a change in the current of the healthy bars, as well as in the behavior and parameters of the motor. In this paper, the method of calculating the rotor bars' current in the SCIM in both healthy and defective states (breakage of one bar and two adjacent bars) is introduced using the multiple coupled circuit (MCC) model. In addition to currents, some important parameters, such as speed and magnetic field, will also be calculated. For validation of results, a two-pole SCIM with a nominal specification of 1.1 kW, 220/380 V, and 50 Hz is subjected to experimental testing. The results are confirmed by practical tests and simulations using the Ansys Maxwell software.

I. Introduction

Squirrel cage induction motors (SCIMs) are widely used in industrial applications due to their simplicity, low cost, easy maintenance, high efficiency, and reliability [1-2]. IM failures lead to significant process delays, increased maintenance costs, and lost revenue. Therefore, implementing predictive maintenance is crucial for identifying the root causes of these failures [3]. Types of faults in induction motors (IMs) include faults related to the stator winding, faults related to bearings, faults related to the rotor, and finally, faults related to external devices. These faults result in unexpected motor failures and substantial costs for the production department [4-6]. Consequently, it is crucial to regularly monitor the condition of IMs. Understanding a machine's electrical, magnetic, and mechanical behavior is essential for reliable condition monitoring [7]. Mathematical models are required for accurate motor performance prediction, computer simulation, and fault signature identification [8-10]. Non-destructive testing is vital for investigating faulty motors in both healthy and faulty conditions, and motor performance models are effective tools for this purpose [11]. As shown in Figure 1, the modeling of IMs can be categorized into three main groups: 1. circuit models, such as multiple-coupled circuits [12] and magnetic equivalent circuit models [13]; 2. state space models, including modified d-q models [14]; and 3. finite element method models, which include full FEM and FEM-SS methods [15]. To obtain a complete solution, full FEM solutions require the utilization of a FEM solver for all solution stages. On the other hand, FEM-SS involves using FEM modeling to estimate parameters for a separate simulator. Table I compares these methods. By examining the characteristics of each of these methods, it can be said that the use of MMC modeling for circuit analysis has proven to be highly effective and versatile, capable of accurately modeling a variety of stator and rotor faults, such as BRB, end ring faults, open circuit and short circuit in the stator winding, static and dynamic eccentricity, and even corrosion [16]. Parameterization of an MCC model for IM requires either detailed knowledge of the internal structure and materials of an IM or sophisticated measurement and testing methods. In [17], the modeling parameters are automatically determined and optimized using measurement data from standard operation with a differential evolution algorithm.

The method is primarily oriented toward practical suitability for industrial applications. The multilevel approach allows for the simulation of the dynamic behavior of unknown IMs. The parametric modeling can then be used to diagnose and identify fault cases. [18] presents a method for coupled electromagnetic and dynamic modeling of an IM with a BRB. It involves creating an MCC model of the IM, a dynamic model of the rotor, and addressing the interaction between these two models. Dynamic simulations and analyses are conducted to investigate the effects of the BRB fault on both the electromagnetic and dynamic characteristics of the IM. [19] presents a model of an SCIM with BRB, utilizing MCC. This analytical model encompasses all spatial harmonic components of the air-gap magnetic force, allowing for an examination of the machine's transient behavior. Equivalent circuits (EC) compatible with both healthy and faulty squirrel-cage rotor topologies are developed. In the EC for a healthy rotor, placing an independent current source in the bar that breaks in the

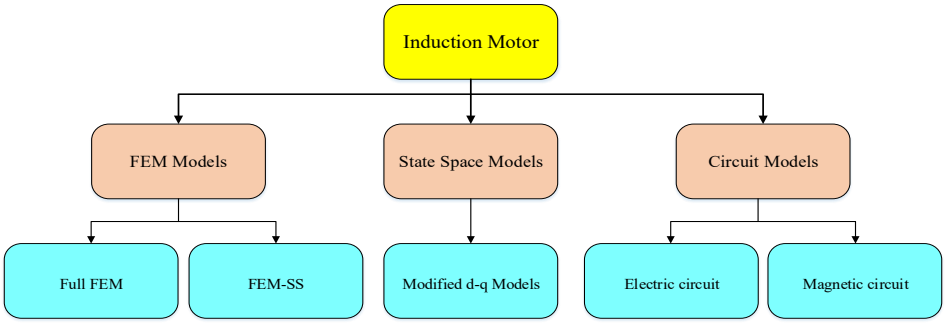

Fig. 1. Types of IM modeling methods

TABLE I COMPARISON OF COMMON IM MODELING METHODS

Method	Advantage	Disadvantage
Multiple coupled circuit (MCC)	• Non-uniform air gap • Practical winding functions • Saturation can be defined in analytical terms. • Different types of faults can be simulated. • The computation time is significantly lower Compared to the FEM. • It strikes a great balance between complexity and accuracy.	• Some geometric constraints, such as those for cooling ducts in the stator or rotor, are difficult to manage.
d-q modeling	• Simple • Comprehensive • Provides good equations for parameter estimation • Good for control and drives	• Negligible saturation • Uniform air gap • Sinusoidal stator winding • No inter-bar currents • No spatial harmonics • No eccentricity faults • No skin effects • Dealing with asymmetries, which are inevitable when a fault occurs, can be quite challenging.
Magnetic equivalent circuit (MEC)	• Spatial dependencies can be included. • Computationally less intense than FEM but more than MCC • It can include geometry, material parameters, and winding distribution	• As all slots must be modeled and the faulty machine is no longer symmetrical, the model becomes quite complex.
Finite element method (FEM)	• Complex geometries can be considered • Non-linearity, such as saturation, skinning effect, and non-idealities can be considered • All types of faults can be simulated; combining FEM with analytical modeling is a good approach.	• The computational complexity is the main issue, particularly in fault diagnostics where symmetry is absent. This problem worsens with 3D analysis and makes it unsuitable for hardware-in-the-loop environments and inverse problem theory.

damaged rotor—whose current is the negative of the current through the same bar—and replacing all voltage sources in the remaining bars with short circuits results in an EC that can be used to resolve the deviations in the rotor mesh currents caused by the bar breakage. Depending on the type of fault, the model parameters can be adjusted to match the machine's behavior. This allows the fault severity to be estimated from the model parameters. Classical models based on the Clark transform are unable to reproduce asymmetric fault conditions. For this purpose, models based on modified WFT and MCC are used. These models allow flexible emulation of many different fault conditions and match the machine's behavior over a wide operating range, even in the faulted condition. The developed model has been evaluated using steady-state measurements on a 5.5 kW inverter-fed induction machine [20]. [21] presents an

approach for detecting BRB in an IM based on an MCC. All self-inductances and mutual inductances of the model are calculated based on the WFT. By employing a genetic algorithm (GA), optimized parameters are obtained by minimizing the errors between the experimental results and the simulation results. The comparison of speed and current shows good agreement between the model and the experimental data under healthy conditions. Because faults related to the rotor account for about 20% of all IM faults [22], and given the importance of monitoring the condition of the motor to prevent unexpected failure, the purpose of this paper is to estimate the rotor bars' current in the SCIM under healthy operating conditions and with a BRB fault using WFT and the MCC model. In other words, we intend to measure the impact of BRB on the main parameters of the SCIM, including the current of other rotor bars. For this purpose, a 2-pole SCIM with nominal specifications of 1.1 kW, 220/380 V, and 50 Hz is subjected to experimental testing and 2D FEM analysis. This motor is tested and analyzed under healthy and defective conditions (breakage of one and two adjacent bars). Under these conditions, the current of the rotor bars is calculated.

The rest of the paper is as follows. In section II, the SCIM modeling based on the MCC model is presented. In section III, the modeling of the BRB fault is described. In section IV, the proposed method for calculating the RBC is shown as a flowchart. In section V, the experimental results are examined and compared with the simulation results. In section VI, losses are evaluated in the BRB fault, and finally, in section VII, the conclusion is presented.

II. IM modelling based on the MCC model

The MCC model was initially introduced in [16] to analyze concentrated winding IMs. This model formulates multiple induction circuits by coupling the stator and rotor of an SCIM. Consider an SCIM having m stator circuits and n rotor bars. The rotor cage is assumed to have n equal loops that are equally spaced, each comprising two rotor bars and the connecting parts of the end rings between them. This configuration is illustrated in Figure 2. In the circuit shown in this figure, we use an RL model. Since we focus on low frequencies, we can ignore the capacitance between turns and windings. Once we have the values for the parameters, we can calculate the loop currents using standard circuit analysis techniques [23].

Therefore, the equations of the IM can be written as a vector matrix in equations (1) to (4).

$$V_S = R_S I_S + \frac{d\Lambda_s}{dt} \quad (1)$$

$$V_r = R_r I_r + \frac{d\Lambda_r}{dt} \quad (2)$$

$$\Lambda_s = L_{ss} I_s + L_{sr} I_r \quad (3)$$

$$\Lambda_r = L_{sr}^T I_s + L_{rr} I_r \quad (4)$$

The L_{sr}^T matrix is the transpose of the L_{sr} matrix. Also:

$$I_s = [i_{s1}\ i_{s2} \dots\ i_{sm}]^T \quad (5)$$

$$I_r = [i_{r1}\ i_{r2} \dots\ i_{rn}]^T \quad (6)$$

$$V_s = [v_{s1}\ v_{s2} \dots\ v_{sm}]^T \quad (7)$$

$$[R_s] = \begin{bmatrix} R_s & 0 & \cdots & 0 & 0 \\ 0 & R_s & \vdots & 0 & 0 \\ \vdots & \vdots & \ddots & \vdots & \vdots \\ 0 & 0 & 0 & R_s & 0 \\ 0 & 0 & \cdots & 0 & R_s \end{bmatrix}_{m\times m} \quad (8)$$

$$[R_r] = \begin{bmatrix} 2(r_b+r_e) & -r_b & 0 & \dots & -r_b \\ -r_b & 2(r_b+r_e) & -r_b & \dots & 0 \\ 0 & -r_b & 2(r_b+r_e) & \dots & \vdots \\ \vdots & \vdots & \vdots & \dots & \vdots \\ -r_b & 0 & \dots & & 2(r_b+r_e) \end{bmatrix}_{n\times n} \quad (9)$$

In the case of the squirrel cage rotor, V_r = [O]. To clarify, it should be noted that the currents in the stator and rotor circuits are assumed to be independent. These circuits can then be connected in any way to create the phases of the stator windings, and the configuration of the rotor bars and end rings can be considered. The torque and mechanical equations of the machine are:

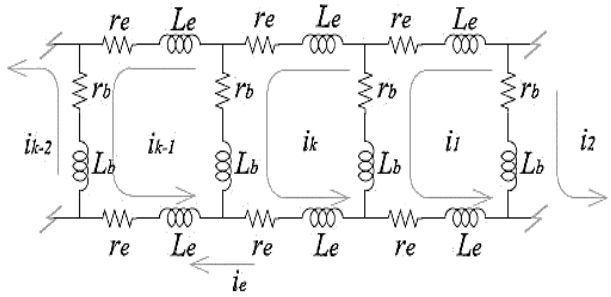

Fig. 2. MCC topology

$$\frac{d\theta}{dt} = \omega \quad (10)$$

$$\frac{d\omega}{dt} = \frac{1}{J}(T_e - T_L) \quad (11)$$

$$T_e = \frac{1}{2} I_s^T \frac{\partial L_{ss}}{\partial \theta_r} I_s + \frac{1}{2} I_s^T \frac{\partial L_{sr}}{\partial \theta_r} I_r + \frac{1}{2} I_r^T \frac{\partial L_{rs}}{\partial \theta_r} I_s + \frac{1}{2} I_r^T \frac{\partial L_{rr}}{\partial \theta_r} I_r \quad (12)$$

where θ is the mechanical angle, ω is the mechanical speed, T_L is the load torque, and J is the rotor inertia.

The calculation of all machine inductances, as indicated by the inductance matrices in the above relations, is the key to a successful simulation of an IM. These inductances are easily calculated using WFT. This method does not assume any symmetry in placing each coil in the slots. According to WFT, the mutual inductance between windings i and j in any electric machine can be calculated using (13) (assuming the permanence of iron is infinite):

$$L_{ij}(\varphi) = \mu_0 r l \int_0^{2\pi} g^{-1}(\varphi.\theta) N_i(\varphi.\theta) N_j(\varphi.\theta) d\theta \quad (13)$$

Where φ is the angular position of the rotor relative to the stator reference, θ is a specific angular position along the inner surface of the stator, $g^{-1}(\varphi.\theta)$ is called the inverse of the distance function, which becomes l/g assuming the air gap is uniform. l is the stack length and r is the average radius

of the air gap. $N_i(\varphi.\theta)$ is called the winding function. Therefore, it is possible to calculate the RBC using these equations.

The key challenge in the analytical approach of SCIM lies in accurately determining the induced current in the rotor bars of the squirrel cage. This requires a precise estimation of the magnetic flux passing through the rotor surfaces. Moreover, it necessitates the use of a highly precise electrical equivalent circuit, whose elements must be correctly identified and determined [16].

III. BRB modeling

The rotor bars of the SCIM are short-circuited by end rings on both sides. This can be modeled as several resistors of equal size (each bar) in parallel with each other. Therefore, when the BRB occurs, it leads to a sudden increase in the resistance of the rotor to a certain extent. There are different methods to identify the resistance of the BRB. One method of measuring the amount of rotor resistance change with the broken bars is expressed as (14). According to (14), the amount of rotor resistance change depends on the number of BRBs [24-25].

$$\Delta R = \frac{n_b}{\frac{N}{3}-n_b} R_r \tag{14}$$

where R_r is the resistance of the healthy rotor, N is the total number of rotor bars, and n_b is the number of BRB.

As mentioned, the method based on MCC and WFT can be used to model SCIM. Using this model, it is possible to successfully simulate the IM under different conditions without changing the model. Therefore, by ignoring the saturation effect, it is possible to simulate the BRB fault by increasing the resistance of the broken bar. The greater the resistance, the greater the severity of the fault. It is sufficient to increase the resistance of the bar to several times its initial value to model the BRB fault [26]. [27] To model an initial fault (a partial BRB), the resistance of the defective bar has been increased. A 10-fold increase in the resistance of the bar creates a similar effect to that of a complete BRB. A 3.5-fold increase is used to simulate a partial BRB fault.

IV. Proposed method for calculating the RBC

The IM's dynamic simulation involves solving the differential equations (1), (2), (10), and (11) together. Various methods can be employed for this purpose. This section describes a relatively simple method. Assuming that the simulation time step (Δt) is chosen to be small enough, these equations can be well approximated in the form of differential equations as follows:

$$[\Lambda_s]_i = \{[V_S]_i - [R_S][I_S]_{i-1}\}\Delta t + [\Lambda_s]_{i-1} \tag{15}$$

$$[\Lambda_r]_i = -[R_S][I_S]_{i-1}\Delta t + [\Lambda_r]_{i-1} \tag{16}$$

$$\omega_i = \frac{1}{J}(\mathrm{T}_{e.i-1} - \mathrm{T}_{L.i})\Delta t + \omega_{i-1} \tag{17}$$

$$\theta_{r.i} = \omega_i \Delta t + \theta_{r.i-1} \tag{18}$$

Also, (3) and (4) can be expressed in terms of the current vectors as follows:

$$[\mathrm{I}_r]_i = ([\mathrm{L}_{rr}]_i - [\mathrm{L}_{sr}]_i{}^T[\mathrm{L}_{ss}]_i{}^{-1}[\mathrm{L}_{sr}]_i)^{-1} \times ([\Lambda_r]_i - [\mathrm{L}_{sr}]_i{}^T[\mathrm{L}_{ss}]_i{}^{-1}[\Lambda_s]_i) \tag{19}$$

$$[\mathrm{I}_s]_i = [\mathrm{L}_{ss}]_i{}^{-1}[\Lambda_s]_i - [\mathrm{L}_{ss}]_i{}^{-1}[\mathrm{L}_{sr}]_i[\mathrm{I}_r]_i \tag{20}$$

The simulation process depicted in Figure 3 begins with the initial step, followed by a loop of simulation stages. During each stage, the parameters and variables of the IM are calculated using the given equations. This loop repeats until the end of the simulation time. The simulation method described here is similar to the numerical solution of state equations and can be accomplished by using software codes such as MATLAB. The proposed method, utilizing numerical and iteration-based techniques with stator data and motor nominal specifications, has a higher convergence speed and accuracy than the conventional MCC method. This is confirmed by the results of Maxwell software simulations based on the FEM method. In the governing equations of the proposed model, considering that the motor power is low and the saturation effect is insignificant, the saturation effect has been ignored to reduce computational load and increase the convergence speed of the proposed model. The advantages and disadvantages of the proposed method are presented in Table II.

The proposed model has the potential to be used in industrial motors and is not limited to a specific power range; in this respect, it is completely scalable.

In this model, given that it focuses more on modeling steady-state conditions of the motor to increase the accuracy of calculations and to consider the effect of increasing motor temperature in steady-state, based on (21) and motor temperature changes in these conditions, this effect has been applied as a coefficient to the constant values of the resistors [28].

$$R_{new} = R_0(1 + \alpha\Delta\theta) \tag{21}$$

where, α is the temperature coefficient of copper or aluminum, Δθ is the temperature change.

Also, in order to consider the effect of skewed rotors in the proposed model, the skew factor approach has been used. In this method, a skew factor is applied to the mutual inductance. This factor is given by (22) [29].

$$K_{skew} = \frac{\sin(\alpha_{skew}/2)}{\alpha_{skew}/2} \tag{22}$$

$$L_{sr.eff} = K_{skew} L_{sr0} \tag{23}$$

V. Simulation results

A SCIM, whose parameters are given in Table III, is investigated in this paper. The stator winding connection is Y. The simulation results are obtained using a balanced three-phase power supply of 380 V, 50 Hz, and under a load of 3.5 Nm (full load). It should be noted that the calculations

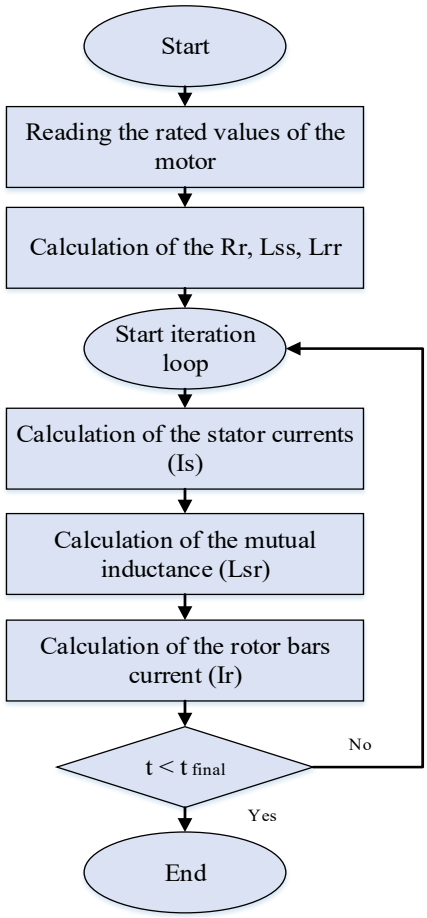

Fig. 3. Flowchart of the calculation process of rotor bars' current

TABLE II ADVANTAGES AND DISADVANTAGES OF THE PROPOSED METHOD

Advantages	Disadvantages
It is Suitable for real-time calculation of the RBC as well as online fault diagnosis	Noise or sensor inaccuracies effect on the RBC calculation.
It is easily implemented on DSPs because they are based on differential equations.	Ignoring the skin effect, hysteresis losses and eddy current at high frequencies
It is straightforward and directly provides information about the IM under different operating conditions.	High sensitivity to changes in motor parameters, including changes in resistances due to temperature changes, changes in inductances due to magnetic saturation.
It uses a smaller number of sensors and only standard variables (voltage, current, and speed).	
It is capable of operating under various loading conditions.	
It can be used for industrial motors with different rated power or number of poles.	
It can model any type of stator and rotor winding structure.	

of the proposed model focus more on the steady-state conditions of the motor and do not examine the start-up transient conditions. Therefore, the results presented in this section are the results of the steady state of the motor. This model performs under different loading conditions, and there are no limitations in this regard. In this section, as an example, the results of the proposed model under nominal load (3.5 N·m) are presented. As shown in Figure 4, this motor is evaluated and tested under both healthy and faulty conditions with a BRB fault (one and two adjacent bars). Figure 5 shows a picture of the laboratory setup. Additionally, to confirm the experimental results, the simulation results of this motor have been obtained using Ansys Maxwell software based on FEM.

A) Matrices of Self and Mutual Inductance

After calculating the inductance matrices based on a method involving repetition by solving the dynamic equations, the stator winding current, the mutual inductance of the stator windings and the rotor bars (L_{sr}), and finally the RBC are calculated.

TABLE III CHARACTERISTICS OF THE STUDIED SCIM

Parameter	Specifications
Power (kW)	1.1
Voltage (V)	380
Frequency (Hz)	50
Speed (RPM)	2850
Nominal Current (A)	2.46
Pole number	2
Number of stator slot	18
Number of rotor bars	16
Air gap length (mm)	1
The inner diameter of the stator core (mm)	67
The outer diameter of the stator core (mm)	121
Number of conductors per stator slot	85
Stator core length (mm)	76
Skew angle of rotor bars (degrees)	5

(a) (b) (c)

Fig. 4. Squirrel cage rotor: (a) healthy (b) 1 broken bar (c) 2 broken bars

According to the proposed method (Figure 4) to calculate the RBC at full load (3.5 Nm) under different conditions, the matrices of self-inductances include the inductance of the stator windings (L_s) and the inductance of the rotor bars (L_r). Additionally, the mutual inductance matrices of the stator windings and the rotor bars have been calculated in the BRB condition, with one BRB (bar number 1) and two BRBs (bars

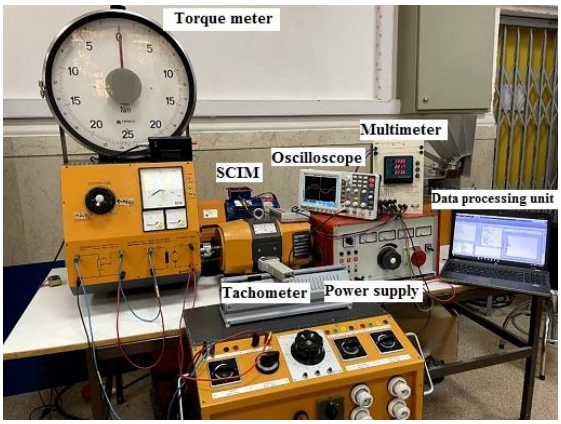

Fig. 5. Laboratory set to calculate the rotor bars' current

number 1 and 2). To validate the experimental results, the results of Ansys Maxwell software have been used.

B) Stator Winding Current

The results of calculating the stator current (Phase A) in a healthy condition, with one BRB (bar number 1), and with two BRBs (bars number 1 and 2) under nominal voltage and full load (3.5 Nm) are shown in Figure 6. The results of the laboratory test measurement of the stator current under the above conditions are equal to 3.5, 4, and 1.4 amps, respectively.

C) Rotor Bars Current

After calculating the matrices of inductance and stator current, the magnitude of RBC under different conditions at time t = 180 ms is presented in Figure 7. As an illustration, Figure 8 displays the current curve for rotor bar number 8. When a BRB fault arises in a rotor, the resistance of the damaged bars increases significantly compared to the resistance of the healthy bars. Figure 7 illustrates that when there are broken bars, some rotor currents flow into the adjacent bars instead of the broken bars due to high resistance, causing an uneven distribution of rotor currents. When a rotor experiences a broken bar, the current in the adjacent bars increases. However, the total current in the rotor is less than what flows through an undamaged rotor. The high current density in the affected bars leads to overheating, which can cause a number of issues, including fluctuations in torque and speed, increased noise, unstable stator currents, and reduced average torque [30].

The sensitivity of the proposed model to changes in the resistance value of the rotor bars is notable. In this model, a 5-fold increase in the bar resistance produces a similar effect to complete BRB, and a 2-fold increase in the bar resistance produces a similar effect to partial BRB. As an example, the current of one of the rotor bars (bar number 8) for a 5-fold increase (complete BRB), a 2-fold increase (partial BRB), and a 10-fold increase at full load (3.5 Nm) is shown in Figure 9.

D) Evaluation of Other Characteristics of the Motor

When the BRB fault occurs, it causes a significant imbalance in the magnetic field within the air gap. As a result, rotating flux harmonics are generated, which consume a considerable amount of reactive power. This reactive power can be greater than the active power, thereby reducing the motor's torque. Rotor faults in IMs generally originate from a minor break in the rotor bar or a point of high resistance. Once such a fault spreads, the magnetic field becomes increasingly asymmetric because of the lack of induced current in the broken bars. This can lead to uneven magnetic distribution and saturation in the stator and rotor teeth near the broken bars, resulting in high harmonic components that can cause electromagnetic issues such as reverse magnetic field generation, torque ripples, and unbalanced magnetization. In Figure 10, you can see the curve of the magnetic flux density in the air gap, which was obtained from the motor models in both healthy and faulty conditions. Figure 11 compares the harmonic components of the magnetic flux density in the air gap. When the rotor is in a healthy state, the THD is equal to 17%, while that of the rotor with one broken bar and two broken bars is equal to 25% and 28%, respectively.

The electromagnetic force is calculated by averaging torque in the simulation. The radial electromagnetic forces (F_r) are computed using Maxwell's stress tensor in (27).

$$F_r = \frac{1}{2\mu_0}(B_n^2 - B_t^2) \quad (27)$$

where B_n and B_t represent the radial and tangential components of the magnetic flux density, μ_0 is vacuum magnetic permeability. The electromagnetic torque is determined by integrating T over the stator and rotor surfaces [31]. Radial electromagnetic forces are shown in Figure 12. The results show that under defective conditions, the level of these forces increases greatly compared to healthy conditions. While the average of these forces is in a healthy state, the rotor with 1 broken bar and the rotor with 2 broken bars have values equal to 0.5, 67, and 152 newtons, respectively. This condition indicates that the areas of the broken bars are subjected to more force, which raises the likelihood of their breakage. If the level of these forces increases, it will result in more electromagnetic noise in the motor.

The speed and torque curves for different motor conditions are shown in Figures 13 and 14, respectively. It can be seen from the comparison of the speed curves that the speed in defective conditions decreases with the increase in the number of BRBs. Also, the speed of the motor in its steady state in healthy and faulty conditions was measured by the tachometer, yielding values of 2791, 2740, and 2720 rpm, respectively. Furthermore, in the torque curves, it can be observed that the torque obtained from the motor with 1 broken bar and 2 broken bars results in a decrease of 10% and 17%, respectively, compared to the healthy motor. Therefore, it can be concluded that with the increase in the

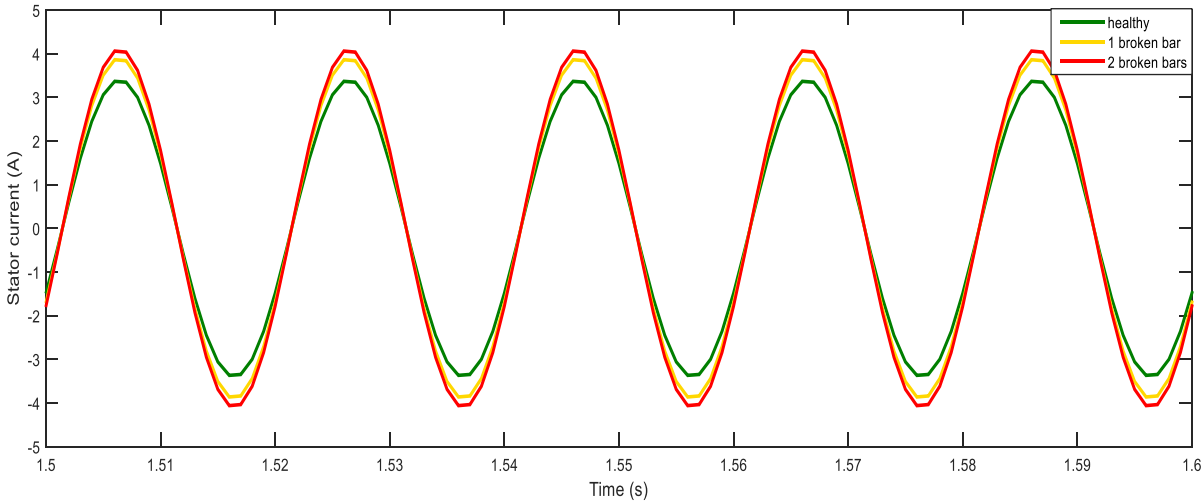

Fig. 6. Stator current (phase A) in different operating conditions

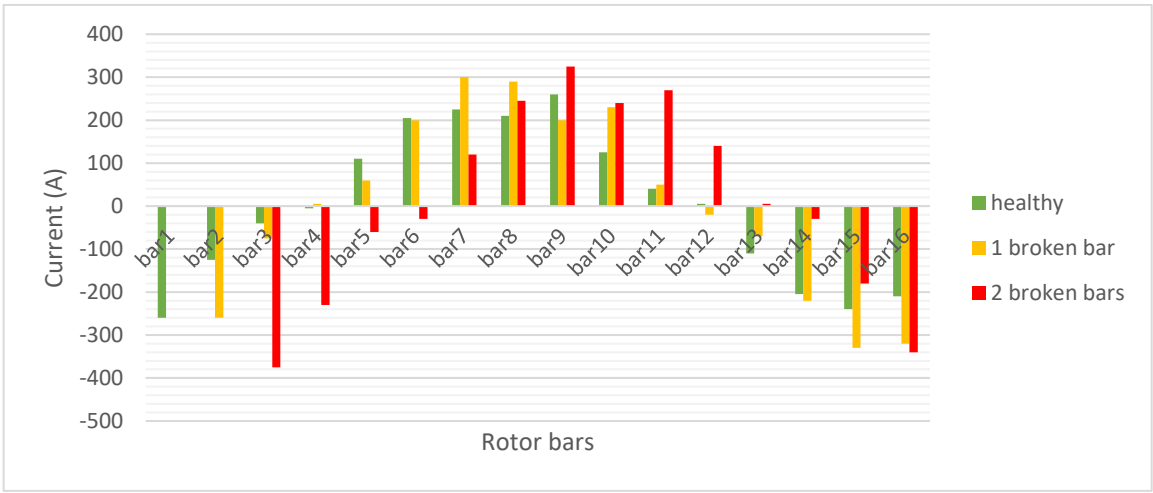

Fig. 7. Magnitude of rotor bars current in healthy and faulty conditions

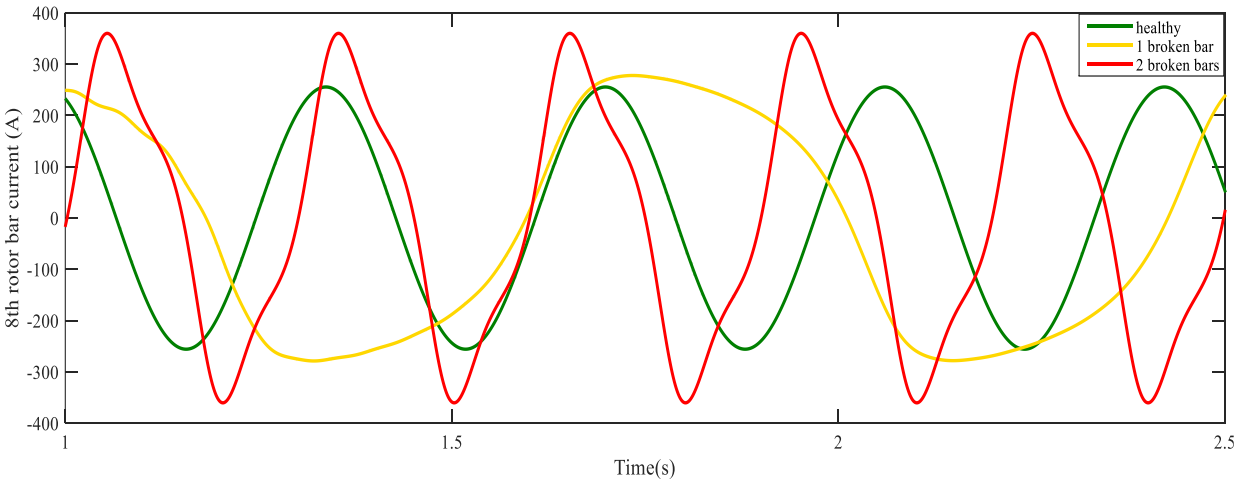

Fig. 8. The current of rotor bar number 8 in healthy and faulty conditions

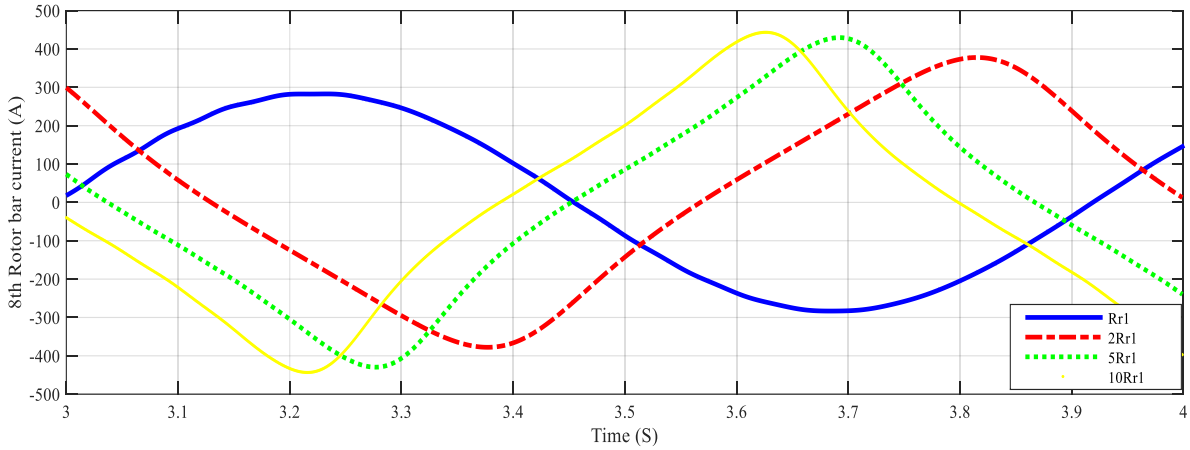

Fig. 9. The current of rotor bar number 8 under conditions of increasing the resistance of rotor bar number 1 by 2, 5 and 10 fold.

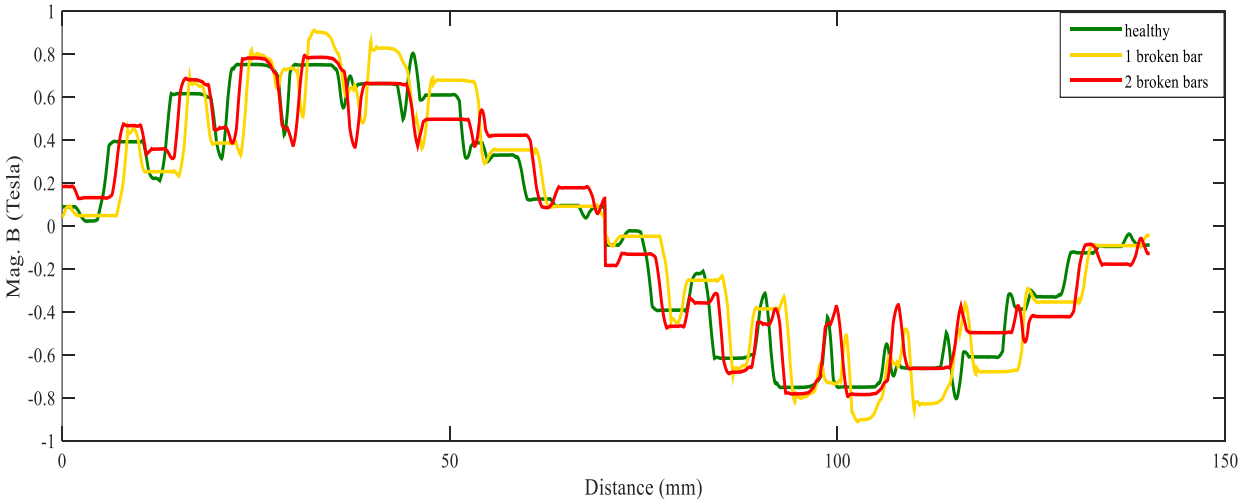

Fig. 10. Flux density distribution curve in healthy and defective conditions

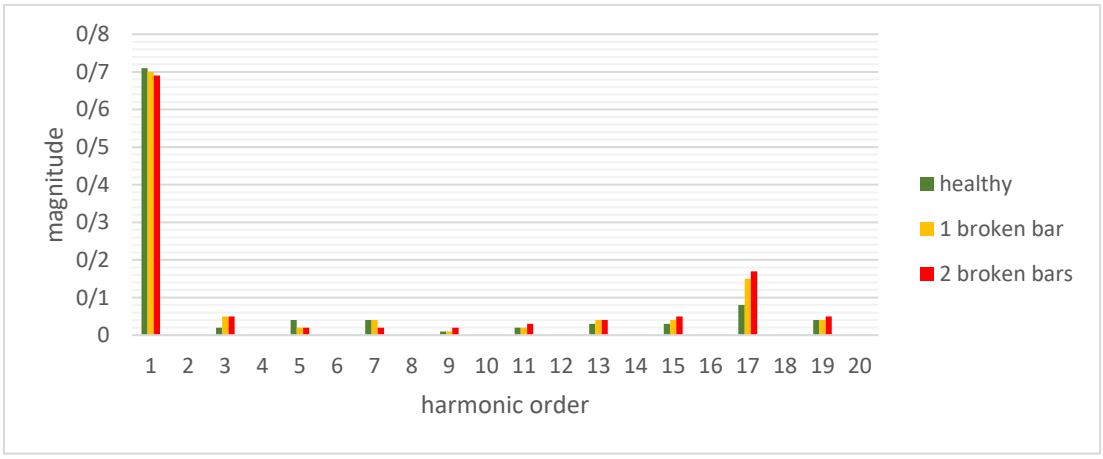

Fig. 11. Comparison of harmonic components of flux density in healthy and defective conditions

number of broken bars, the values of speed and torque decrease. The torque ripple in healthy conditions, with a rotor having 1 broken bar, and with a rotor having 2 broken bars, was measured as ±0.4, ±0.5, and ±0.7, respectively

.

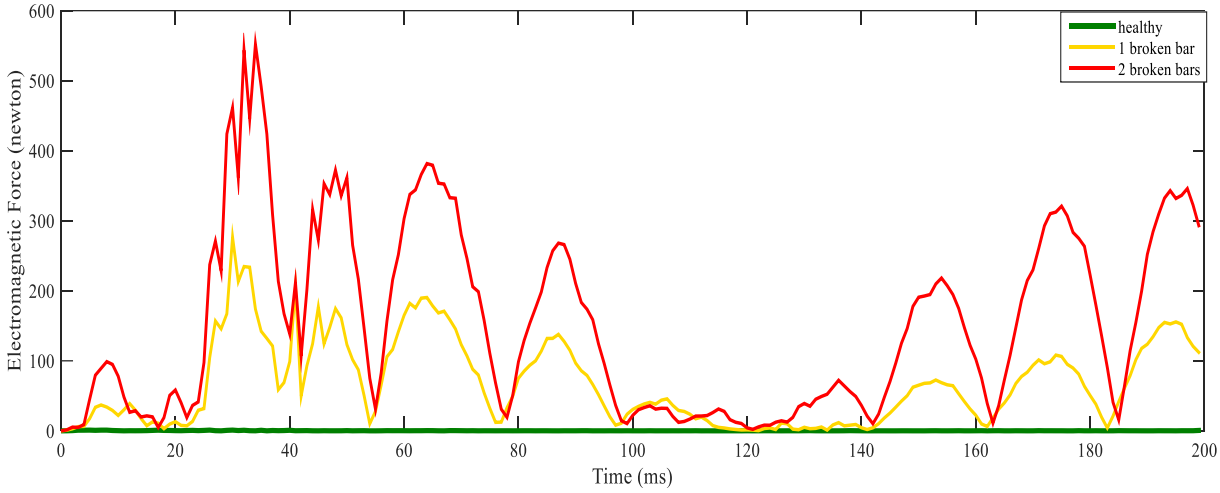

Fig. 12. Radial electromagnetic force in healthy and defective conditions

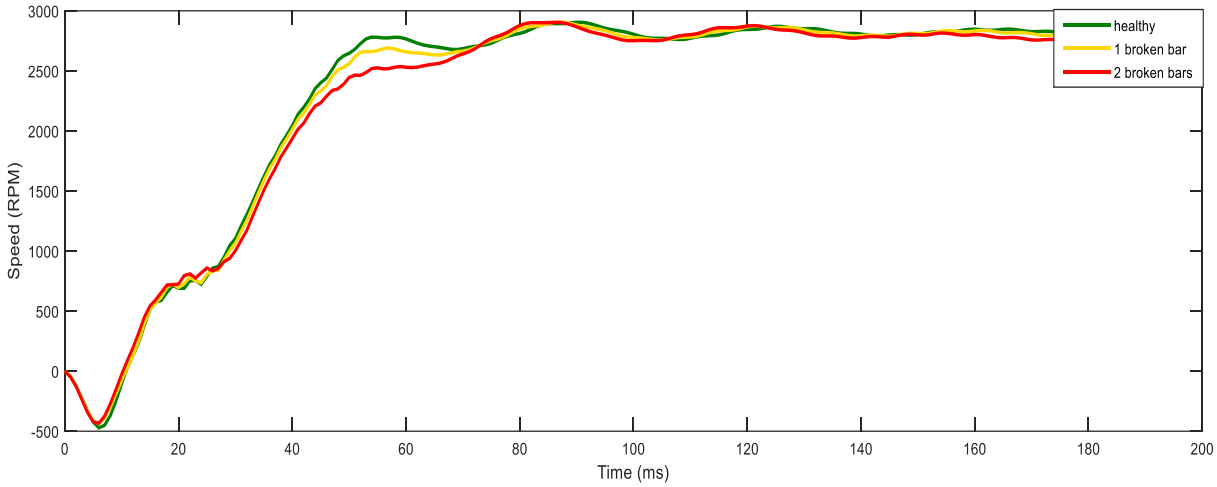

Fig. 13. Rotor speed in healthy and defective conditions

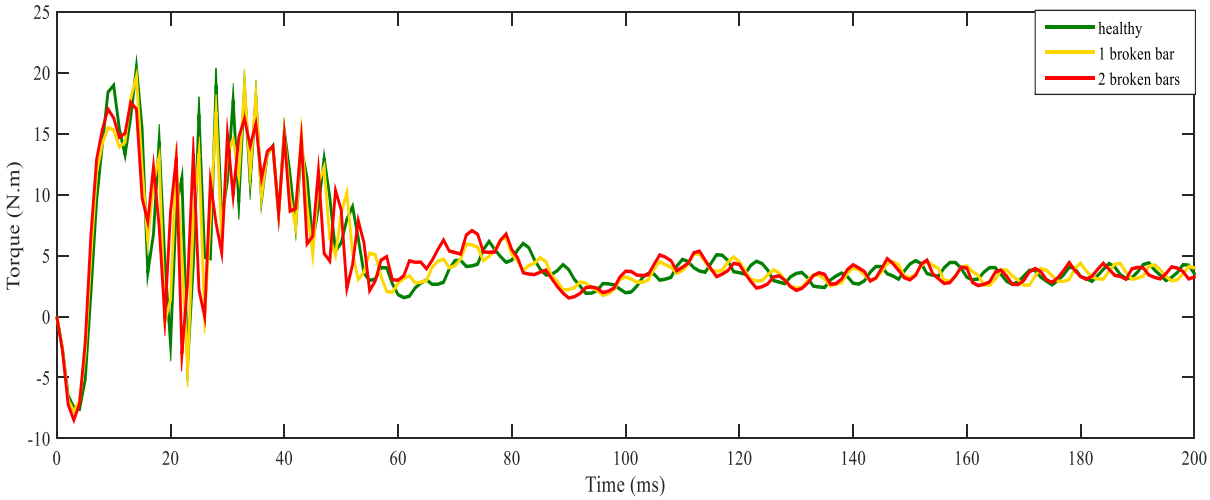

Fig. 14. Torque in healthy and defective conditions

VI. Losses in the BRB fault

The losses in an IM include constant losses and variable losses. Constant losses are those that remain constant in the normal operating range of the motor, and their value does not change. These losses include iron losses (core losses), friction losses, and windage losses, which can be calculated by performing a no-load test. Variable losses are also referred to as copper losses. These losses include stator copper losses and rotor copper losses. Copper losses can also be calculated by performing a blocked rotor test. A no-load test (Figure 15) and a blocked rotor test (Figure 16) have been performed on the studied motor. By using the DC test, the resistance of each stator phase can be calculated. The results of these tests on a healthy motor under nominal conditions are presented below. It is important to note that the presence of a BRB can have a significant effect on the efficiency of an SCIM. Due to broken bars, the motor losses increase, and some of the rotor bars may become overloaded. This overload can cause an increase in inter-bar currents that flow from the rotor core between the broken bar and adjacent bars. This can compromise the motor's efficiency. However, there is limited literature available on this particular effect [32-33]. It's worth exploring the effects of non-adjacent bar breaking in addition to other factors. While this is a less common occurrence, some studies have found that non-adjacent bars in the rotor cage can break under certain conditions [34-35]. In such situations, diagnosing the fault becomes challenging, as existing techniques like motor current analysis may not be effective. This is because the impacts of different breaks can be compensated for to some extent, depending on the relative position of the bars that have broken.

According to the DC test, the results of the no-load and blocked rotor tests of the Y-connected motor are presented in Tables IV and V, respectively. Based on the results of the DC test, no-load test, and blocked rotor test, motor losses are calculated and shown in Table VI. Additionally, the efficiency of the motor under healthy and BRB fault conditions are calculated and presented in Table VII. As can be seen, depending on the severity of the fault, the efficiency is affected, and this value decreases. Furthermore, iron and copper losses are compared in Table VIII.

In Table IX, experimental and simulation results are compared. In this table, the currents of rotor bars numbers 8 and 16, obtained from experimental and simulation results, have been compared. Rotor bar number 8 is the farthest from the BRBs (rotor bars numbers 1 and 2), while rotor bar number 16 is located near the BRBs. Additionally, the losses and efficiency of the motor under different conditions have been compared.

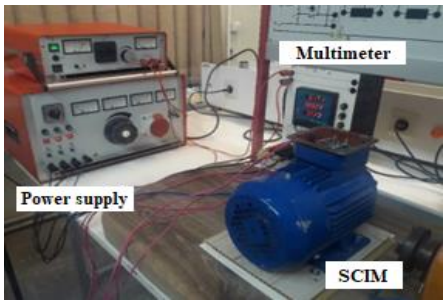

Fig. 15. No-load test laboratory set

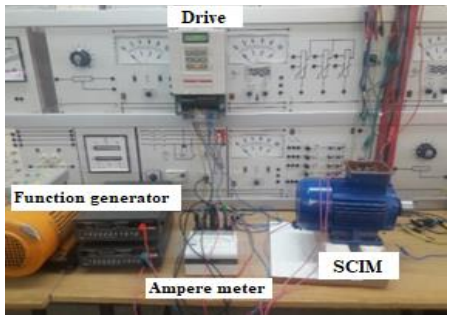

Fig. 16. Blocked rotor test laboratory set

TABLE IV NO LOAD TEST RESULTS

Parameter	Phase A	Phase B	Phase C
Active power (W)	70	65	50
Reactive power (VAR)	168	145	150
Voltage (V)	380	380	380
Current (A)	1.17	1	1.1
Power factor	0.27	0.24	0.19

TABLE V BLOCKED ROTOR TEST RESULTS

Parameter	Active power (W)	Reactive power (VAR)	Voltage (V)	Current (A)	Frequency (Hz)
Specifications	40	20	85	2.46	12

TABLE VI BLOCKED ROTOR TEST RESULTS

Parameter	Active power (W)	Reactive power (VAR)	Voltage (V)	Current (A)	Frequency (Hz)
Specifications	40	20	85	2.46	12

TABLE VII LOSSES OF THE STUDIED MOTOR

Losses	Core losses	Stator copper loss	Rotor copper loss
Specifications	85	136	48

TABLE VIII ELECTROMECHANICAL CHARACTERISTICS OF THE MOTOR IN THE DIFFERENT OPERATING CONDITIONS UNDER NOMINAL CONDITIONS

Conditions	Phase voltage (V)	Phase current (A)	Power factor	Torque (Nm)	Speed (RPM)	Mechanical power (kW)	Electrical power (kW)	Efficiency (%)
Healthy	220	2.5	0.92	3.5	2795	1.03	1.30	80.02
1 BRB	220	3.12	0.91	3.5	2740	1	1.33	75.18
2 BRBs	220	3.28	0.91	3.5	2720	0.996	1.38	71.73

TABLE IX LOSSES IN THE DIFFERENT OPERATING CONDITIONS UNDER NOMINAL CONDITIONS

Conditions	Stator copper loss (W)	Rotor copper loss (W)	Core losses + Windage losses (W)
Healthy	136	48	85
1 BRB	170	54	105
2 BRBs	197	71	112

TABLE X COMPARISON OF EXPERIMENTAL AND SIMULATION RESULTS

Parameter	Experimental results			Simulation results		
	Healthy	1 BRB	2 BRBs	Healthy	1 BRB	2 BRBs
stator current(A)	3.3	3.8	3.9	3.45	3.92	4.07
current bar number 16 (A)	230	260	310	235	268	312
current bar number 8 (A)	230	240	260	235	242	263
Torque ripple(N.m)	± 0.4	± 0.5	± 0.7	± 0.6	± 0.8	±1.1
Losses (W)	270	329	380	230	303	253
Efficiency (%)	79.23	75.18	72.46	83.57	82.35	80.55

VII. Conclusion

In this paper, a method for calculating the RBC in an SCIM under healthy and faulty conditions was presented. A key strength of the proposed approach is that it enables direct and precise estimation of individual rotor bar currents using the MCC model, which provides deeper insight into motor behavior under broken bar faults compared with conventional analysis. The results demonstrated that the presence of one or two broken bars significantly alters the motor's performance. The stator current increased from about 3.3 A in the healthy case to nearly 3.9 A with two broken bars, while efficiency dropped from approximately 80% to 72%. Furthermore, rotor and stator copper losses increased noticeably, and the motor speed decreased slightly (around 75 RPM). These variations indicate higher thermal and electrical stress on the remaining healthy bars and the overall motor. Finally, the close agreement between experimental measurements and simulation results confirms the accuracy of the MCC model and the reliability of the proposed analysis.

Conflicts of Interest: The authors declare that there is no conflict of interest regarding the publication of this paper.

References

[1] Shadfar, Hamed, and Hamid Reza Izadfar. "A New Squirrel Cage Rotor Structure to Improve the Dynamic Performance of the Single Phase Induction Motor." *International Journal of Industrial Electronics Control and Optimization, Vol.* 5, No. 4, pp. 279-286, 2022.

[2] Niaz Azari, Milad, Vasiye Lohrasbi, and Seyed Abdolah Mousavi. "Optimum design of high-temperature superconducting induction/synchronous motor to increase torque density using collective decision optimization algorithm." International Journal of Industrial Electronics Control and Optimization, Vol. 3, No. 2, pp. 137-145, 2020.

[3] Prasad, Kapu V. Sri Ram, and Varsha Singh. "Fault Diagnosis of Induction Machine for Rotor Cage Damage Using MCSA for Industrial Application." Electric Power Components and Systems, pp. 1-13, 2024.

[4] Bahgat, Bahgat Hafez, E. A. Elhay, Tole Sutikno, and Mahmoud M. Elkholy. "Revolutionizing motor maintenance: a comprehensive survey of state-of-the-art fault detection in three-phase induction motors." *International Journal of Power Electronics and Drive Systems,* Vol.15, No. 3, pp. 1968-1989, 2024.

[5] Dehnavi, Vahid Safari, and Masoud Shafiee. "Fault diagnosis of induction motors using novel measurement techniques and data fusion." *Measurement* (2025): 118135.

[6] Wang, Bingnan. "Induction Motor Fault Classification with Topological Data Analysis." In *2024 IEEE Energy Conversion Congress and Exposition (ECCE)*, pp. 5381-5386, 2024.

[7] Sheikh, Muhammad Aman, Sheikh Tahir Bakhsh, Muhammad Irfan, Nursyarizal bin Mohd Nor, and Grzegorz Nowakowski. "A review to diagnose faults related to three-phase industrial induction motors." *Journal of Failure Analysis and prevention,* Vol.22, No. 4, pp. 1546-1557, 2022.

[8] Gundewar, Swapnil K., and Prasad V. Kane. "Condition monitoring and fault diagnosis of induction motor." *Journal of Vibration Engineering & Technologies,* Vol. 9, pp. 643-674, 2021.

[9] Kavitha, M. "Hybrid AI-Mathematical Modeling Approach for Predictive Maintenance in Rotating Machinery Systems." *Journal of Applied Mathematical Models in Engineering*, pp. 1-8, 2025.

[10] AlShorman, Omar, Muhammad Irfan, Ra'ed Bani Abdelrahman, Mahmoud Masadeh, Ahmad Alshorman, Muhammad Aman Sheikh, Nordin Saad, and Saifur Rahman. "Advancements in condition monitoring and fault diagnosis of rotating machinery: A comprehensive review of image-based intelligent techniques for induction motors." *Engineering Applications of Artificial Intelligence*, Vol. 130, p. 107724, 2024.

[11] Konuhova, Marina. "Induction Motor Dynamics Regimes: A Comprehensive Study of Mathematical Models and Validation." *Applied Sciences*, Vol. 15, No. 3, p. 1527, 2025.

[12] Benninger, M., M. Liebschner, and C. Kreischer. "Automated Parameter Identification for Multiple Coupled Circuit Modeling of Induction Machines." In *2022 International Conference on Electrical Machines (ICEM)*, pp. 1307-1313. IEEE, 2022.

[13] Zhu, Xinkai, Guangyu Qi, Ming Cheng, Wei Qin, Yabin Liu, and Jiwei Huang. "Equivalent magnetic network model of electrical machine based on three elements: magnetic flux source, reluctance and magductance." *IEEE Transactions on Transportation Electrification,* 2024.

[14] Olarinoye, G. A., and I. Abdulwahab. "Comparative analysis and simulation of the dq reference frame model of the three phase induction motor and its modification." *Arid Zone Journal of Engineering, Technology and Environment,* Vol. 18, No. 1, pp. 41-52, 2022.

[15] Prasad, Kapu V. Sri Ram, K. Dhananjay Rao, and Faisal Alsaif. "Induction motor structure design to reduce vibrations with numerical (fea) and experimental (va) techniques." *IEEE Access,* 2024.

[16] X. Luo, Y. Liao, H. Toliyat, A. El-Antably, T. Lipo.: Multiple coupled circuit modeling of induction machines, IEEE Trans. Ind. Appl. Vol. 31, No. 2, pp. 311–318, 1995.

[17] Benninger, M., M. Liebschner, and C. Kreischer. "Automated Parameter Identification for Multiple Coupled Circuit Modeling of Induction Machines." In *2022 International Conference on Electrical Machines (ICEM)*, pp. 1307-1313. IEEE, 2022.

[18] Yang, Yi, Niaoqing Hu, Zhe Cheng, Jiangtao Hu, and Jiao Hu. "Coupled electromagnetic-dynamic modelling of induction motor with a broken rotor bar." In *Ninth International Symposium on Sensors, Mechatronics, and Automation System*, Vol. 12981, pp. 1176-1181, 2024.

[19] Fu, Qiang, Qing Guo, Wei Zhang, Weimin Cui, and Ling Zhao. "An analytical model for squirrel cage induction machine with broken rotor bars derived based on the multiple coupled circuit theory and the winding function approach." *International Journal of Circuit Theory and Applications*, Vol. 49, No. 6, pp. 1633-1658, 2021.

[20] Yu, Xinyi, Stefan Quabeck, Stephan Schüller, and Rik W. De Doncker. "Modelling of broken rotor bars and eccentricity faults in squirrel cage induction machines." In *2021 IEEE 13th International Symposium on Diagnostics for Electrical Machines, Power Electronics and Drives (SDEMPED)*, vol. 1, pp. 133-139. IEEE, 2021.

[21] Wei, C. H., L. Yan, W. H. Tang, and Q. H. Wu. "Detection of broken bars in induction motor based on multiple coupled circuit model with optimized parameters." In *2013 IEEE PES Asia-Pacific Power and Energy Engineering Conference (APPEEC)*, pp. 1-6. IEEE, 2013.

[22] Abdulkareem, Ademola, Tochukwu Anyim, Olawale Popoola, John Abubakar, and Agbetuyi Ayoade. "Prediction of induction motor faults using machine learning." *Heliyon* , Vol.11, No. 1, 2025.

[23] M.S.R. Krishna, K. S. Ravi, "Fault diagnosis of induction motor using motor current signature analysis", in 2013 International Conference on Circuits, Power and Computing Technologies (ICCPCT), pp. 180-186, 2013.

[24] Hussain, Syed Nazim, and Syed Sajjad Haider Zaidi.: Modeling and analysis of a three-phase induction motor with a broken rotor bar. In 17th IEEE International Multi Topic Conference, pp. 488-493, 2014.

[25] Nait-Said, N. "Rotor resistance estimation of an induction motor to detect broken bars fault using HH method." Electric Power Components and Systems, Vol. 32, No. 2, pp. 149-161, 2004.

[26] C. Kral, A. Haumer, and C. Grabner.: Modeling and Simulation of Broken Rotor Bars in Squirrel Cage Induction Machines, Proceedings of the World Congress on Engineering, pp.1 - 3, 2009.

[27] Pezzani, C., G. Bossio, and C. De Angelo.: Winding distribution effects on induction motor rotor fault diagnosis. Mechatronics, Vol. 24, No.8, pp.1050-1058, 2014.

[28] Khalifa, Fahim A., Sobhy Serry, Mohamed M. Ismail, and Basem Elhady. "Effect of temperature rise on the performance of induction motors." In 2009 International Conference on Computer Engineering & Systems, pp. 549-552. IEEE, 2009.

[29] A. Tessarolo, R. Menis, "Influence of Skewing on the Harmonic Content of Induction Machine Torque", Electric Power Systems Research, pp.45-56, 2018.

[30] Yektaniroumand, T., M. Niaz Azari, and M. Gholami. "Optimal rotor fault detection in induction motor using ppaper-swarm optimization optimized neural network." International Journal of Engineering, Vol.31, No.11, pp.1876-1882, 2018.

[31] El Idrissi, Abderrahman, Aziz Derouich, Said Mahfoud, Najib El Ouanjli, Ahmed Chantoufi, and Youness El Mourabit. "Acoustic characterization of a three-phase asynchronous machine under stator unbalance defects." *e-Prime-Advances in Electrical Engineering, Electronics and Energy*, Vol. 12, p. 100958, 2025.

[32] Imaouchen, Yacine, Samira Chekkal Ait Ouaret, Djamal Aouzellag, and Kaci Ghedamsi. "The Effect of Stator and Rotor Faults on the Dual-star Induction Motor Behavior." *Periodica Polytechnica Electrical Engineering and Computer Science*, Vol. 69, No. 2, pp. 111-121, 2025.

[33] Drobnič, Klemen, Mitja Nemec, Henrik Lavrié, Vanja Ambrožié, and Rastko Fižer. "Detection of Broken Rotor Bars in Presence of Load Oscillations." *IEEE access*, 2025.

[34] G. Y. Sizov, A. Sayed-Ahmed, Y. Chia-Chou, N. A. O. Demerdash.: Analysis and diagnostics of adjacent and nonadjacent broken rotor bar faults in squirrel-cage induction machines. IEEE Trans. Ind. Elec., Vol.56, No.11, pp.4627–4641, 2009.

[35] M. Riera-Guasp, M. F. Cabanas, J. A. Antonino-Daviu, M. Pineda-Sanchez, C. H. R. Garcia.: Influence of nonconsecutive bar breakages in motor current signature analysis for the diagnosis of rotor faults in induction motors, IEEE Trans. Energy Convers., Vol. 25, pp. 80-89, 2010.

Hamed Shadfar received his M.Sc. degree from Semnan University, Semnan, Iran, in 2018 with First class distinction. He is working toward a Ph.D. in the Faculty of Electrical and Computer Engineering, Semnan University, Semnan, Iran. His major research interests include design, modeling, condition monitoring, and fault diagnosis of electric machines.

Hamid Reza Izadfar is currently an Associate Professor in the Electrical and Computer Engineering Department of Semnan University. His main research interests are the design and analysis of electric machines and drives.